A&A 541, A72 (2012)
DOI: 10.1051/0004-6361/201218999

Astronomy & Astrophysics

Milliarcsecond structure of water maser emission in two young high-mass stellar objects associated with methanol masers⋆

A. Bartkiewicz[1], M. Szymczak[1], and H. J. van Langevelde[2,3]

[1] Toruń Centre for Astronomy, Nicolaus Copernicus University, Gagarina 11, 87-100 Toruń, Poland
e-mail: [annan;msz]@astro.uni.torun.pl
[2] Joint Institute for VLBI in Europe, Postbus 2, 7990 AA Dwingeloo, The Netherlands
e-mail: langevelde@jive.nl
[3] Sterrewacht Leiden, Leiden University, Postbus 9513, 2300 RA Leiden, The Netherlands

Received 9 February 2012 / Accepted 12 March 2012

ABSTRACT

Context. The 22.2 GHz water masers are often associated with the 6.7 GHz methanol masers but owing to the different excitation conditions they likely probe independent spatial and kinematic regions around the powering young massive star.
Aims. We compared the emission of these two maser species on milliarcsecond scales to determine in which structures the masers arise and to test a disc-outflow scenario where the methanol emission arises in a circumstellar disc while the water emission comes from an outflow.
Methods. We obtained high-angular and spectral resolution 22.2 GHz water maser observations of the two sources G31.581+00.077 and G33.641−00.228 using the EVN.
Results. In both objects the water maser spots form complex and filamentary structures of sizes 18–160 AU. The emission towards the source G31.581+00.077 comes from two distinct regions of which one is related to the methanol maser source of ring-like shape. In both targets the main axis of methanol distribution is orthogonal to the water maser distribution. Most of water masers appear to trace shocks on a working surface between an outflow/jet and a dense envelope. Some spots are possibly related to the disc-wind interface which is as close as 100–150 AU to the regions of methanol emission.

Key words. stars: formation – ISM: molecules – masers – instrumentation: high angular resolution

1. Introduction

High-angular resolution observations of high-mass star forming sites in the 6.7 GHz methanol maser emission have revealed a diversity of morphological structures from very simple composed of a few milliarcsecond (mas) wide spots to complex and extended clouds of arcsecond sizes (Phillips et al. 1998; Walsh et al. 1998; Minier et al. 2000; Dodson et al. 2004; Bartkiewicz et al. 2009; Pandian et al. 2011). Linear structures with a velocity gradient are thought to be the signature of an edge-on disc or torus around young massive protostars (Norris et al. 1998; Minier et al. 2000) but there is evidence that some of them are associated with outflows (De Buizer 2003) or even a shock propagating through a rotating dense molecular clump (Dodson et al. 2004). Arc-like or ring-like morphologies of methanol emission seem to prove a disc scenario (Bartkiewicz et al. 2009), although most of those structures do not show signs of rotation but rather inflow or/and outflow dominate (van Langevelde et al. 2010), it is then postulated that methanol masers arise in the shock interface between the large scale accretion and a circumstellar disc.

While the 6.7 GHz methanol maser line is radiatively pumped in warm ($T \sim 150$ K) and dense ($n \leq 10^8$ cm^{-3}) regions (Cragg et al. 2005; Sobolev et al. 1997), the 22 GHz water maser emission is collisionally pumped and probes denser ($n \geq 10^8$ cm^{-3}) and hotter ($T \sim 400$ K) gas (Elitzur et al. 1989). The water maser is often excited in strong shocks, driven by young low-mass and high-mass (proto)stellar objects, on a working surface between a outflow and a dense envelope. A number of morphologies of this emission is observed from collimated jet, wide-angle flows, expanding shells to equatorial flows (Goddi et al. 2007; Moscadelli et al. 2007, 2011; Sanna et al. 2010a,b; Torrelles et al. 2011). One or more types of those maser structures occur simultaneously in star forming regions on scale sizes of a few mas to several arcsec and is possibly related to the geometry of the envelopes or the mechanisms driving the outflows.

Our recent VLA survey of 22 GHz water masers in a sample of 31 methanol sources has yielded 22 detections (Bartkiewicz et al. 2011) where both maser species are excited by the same central objects. We noted that a distinct group of methanol sources with ring-like structure show either no associated water masers at all or water masers that are distributed orthogonally to the major axis of the ring. It is argued that the methanol maser structure traces a circumstellar disc/torus around a high-mass young stellar object while the water masers originate in outflows. As the VLA data are of moderate angular and spectral resolutions of ∼1″ and 0.65 km s^{-1}, respectively, we undertook the VLBI observations to examine a disc-outflow scenario in the two brightest water maser targets, which show the arc-like or ring-like morphologies that are characteristic of methanol masers.

The source G31.581+00.077[1] has been recognized as a massive young stellar object based on 6.7 GHz methanol maser observations (Szymczak et al. 2000). The methanol maser spots

⋆ The colour versions of all figures are available on-line.

[1] The names of two targets follow the Galactic coordinates of the brightest methanol maser spots derived by Bartkiewicz et al. (2009).

are distributed along an arc or ring of 217 mas size (Bartkiewicz et al. 2009), which corresponds to ∼1200 AU for the assumed near kinematic distance of 5.5 kpc (Reid et al. 2009). The detection of an infrared source of bolometric luminosity of 3×10^4 $L_\odot$ (Urquhart et al. 2011), 22 GHz H_2O maser emission (Bartkiewicz et al. 2011), 1665 and 1667 MHz weak OH masers (Szymczak & Gérard 2004), millimeter molecular thermal lines (Szymczak et al. 2007; Urquhart et al. 2008), and 5 and 8.4 GHz continuum emission at location of 31.582+00.075 (i.e., 9″ apart from the maser arc/ring) (Urquhart et al. 2009; Bartkiewicz et al. 2009) indicates that this is a cluster of recent star formation.

The source G33.641−00.228 detected in the 6.7 GHz methanol line (Szymczak et al. 2000) has an arc spot distribution of length 630 AU (Bartkiewicz et al. 2009) for the assumed near kinematic distance of 3.8 kpc (Reid et al. 2009), which seems to be more likely than the far kinematic distance (Zhang, priv. comm.). The site also contains water and OH masers (Bartkiewicz et al. 2011; Szymczak & Gérard 2004) but no 8.4 GHz continuum emission was detected with an upper limit of 0.15 Jy (Bartkiewicz et al. 2009). The detection of radio recombination lines at about 103 km s^{-1} (Anderson et al. 2011) and a multi-feature ^{13}CO line spectrum (Urquhart et al. 2008) illustrates the complexity of this molecular cloud and its clustered star formation.

2. Observations and data reduction

The EVN[2] observations of G31.581+00.077 and G33.641−00.228 with the antennas at Jodrell Bank, Effelsberg, Medicina, Metsähovi, Onsala, and Yebes, were carried out at 22.23508 GHz on 2010 October 30 for 8 h (the project EB047). The tracking phase centres were estimated from the VLA survey for the water maser spots that were located nearest to the methanol emission in each target (Bartkiewicz et al. 2011) at $\alpha = 18^{\rm h}48^{\rm m}41\overset{\rm s}{.}951$, $\delta = -01^\circ10'02\overset{''}{.}578$ and $\alpha = 18^{\rm h}53^{\rm m}32\overset{\rm s}{.}563$, $\delta = +00^\circ31'39\overset{''}{.}130$ (J2000), respectively. A phase-referencing scheme was applied with a reference source J1851+0035 (from the VLA calibrator catalogue), using a cycle time between the maser and phase-calibrator of 60 s+90 s. This strategy yielded 2 h on-source times for each target. The bandwidth was set to 8 MHz and data were correlated with the Mk IV Data Processor operated by JIVE with 1024 spectral channels. The resulting spectral resolution was 0.1 km s^{-1}. The velocity was measured with respect to the local standard of rest (LSR).

The data calibration and reduction were carried out with NRAO's Astronomical Image Processing System (AIPS) using standard procedures for spectral line observations. We used the Effelsberg antenna as a reference. The amplitude was calibrated by performing measurements of the system temperature at each telescope and applying the antenna gain curves. The parallactic angle corrections were subsequently added to the data. The source 3C 454.3 was used as a delay, rate, and bandpass calibrator. The phase-calibrator was imaged and a flux density of 190 mJy was obtained. The maser data were corrected for all Doppler effects and self-calibrated using the brightest and most compact maser spot. Finally, naturally weighted maps of spectral channels were created in the velocity range where the emission was seen in the scalar-averaged spectrum. For imaging, the resulting synthesized beam was 1.0 × 2.4 mas^2 with a position angle (PA) of −38°, while the pixel separation was 0.2 mas in both coordinates. The rms noise levels ($1\sigma_{\rm rms}$) in line-free channels was typically 10 mJy beam^{-1}. The weakest detected maser spot had a brightness of 94 mJy beam^{-1} that is more than $9\sigma_{\rm rms}$.

The positions of water maser spots in all channel maps were determined by fitting two-dimensional Gaussian models. The formal fitting errors resulting from the beamsize/signal-to-noise ratio were smaller than 0.1 mas. To determine the position accuracy of registered maser spots, we need to consider the following factors (Diamond et al. 2003): i) the uncertainty in the phase-reference source position of 2 mas[3]; ii) the antenna positions, where the claimed accuracy of ∼1 cm corresponds to 1 mas in RA and 2 mas in Dec; iii) the phase transfer over the separation between targets and the phase-calibrator: 1.°92 (between G31.581+00.077 and J1851+0035) and 0.°45 (between G33.641−00.228 and J1851+0035). These caused potential phase-solution transfer errors corresponding to 1 mas in RA and 2 mas in Dec for G31.581+00.077 and to 0.2 mas in RA and 0.4 mas in Dec for G33.641−00.228, respectively. In total, the absolute position accuracy ($1\sigma_{\rm pos}$) is 2.5 mas in RA and 3.5 mas in Dec for both targets.

3. Results

Water maser emission towards both targets was mapped, after successful phase-referencing, in the areas of 5″× 5″ and the velocity range explored by Bartkiewicz et al. (2011) using the VLA. The EVN maps of water maser spots (Figs. 1 and 3) are overlayed on the VLA maps and the 6.7 GHz methanol maser distributions obtained with the EVN (Bartkiewicz et al. 2009). The *Spitzer* GLIMPSE maps[4] of the 4.5–3.6 μm emission excess are added. Following the procedure described in Bartkiewicz et al. (2009), the water maser spots are analysed to identify individual velocity-coherent maser *clouds*. Their basic parameters, such as positions, ΔRA, ΔDec, LSR velocities, $V_{\rm LSR}$, and intensities of the brightest spot, $S_{\rm p}$, of each cloud are listed in Tables 1 and 2. The water and methanol maser spectra of single clouds are combined in Figs. 2 and 4 with overlays of individual Gaussians, if emission was seen in at least three consecutive channels. A Gaussian analysis of individual clouds is carried out and the fitted flux amplitude, $S_{\rm fit}$, the full width at half-maximum, FWHM, the projected extent between the most separated single spot centres within a cloud, $L_{\rm proj}$, and the velocity gradient, $V_{\rm grad}$ are listed in Table 3. The lower limit to the brightness temperature, $T_{\rm b}$, of each cloud is also calculated according to Eq. (9−27) of Wrobel & Walker (1999). For comparison purposes, the same analysis is done for the 6.7 GHz methanol maser data (Table 3) obtained in 2007 June (G31.581+00.077) or 2003 June (G33.641−00.228) with the EVN. Below we comment in more detail on each source.

3.1. G31.581+00.077

A total of 91 water maser spots were detected. They are concentrated in two distinct regions (Fig. 1). The south-east (SE) region of size 50 × 30 mas^2 containing weak (<1.35 Jy) emission in the velocity ranges from 90.1 to 93.9 km s^{-1} and from 100.0 to 103.3 km s^{-1} is located close to the phase centre. The second region (NW) of middle velocity emission (96.8−100.7 km s^{-1}) and flux density of 2.6−16.5 Jy is located offset by ∼5″ to the north-west (PA = −60°) of the phase centre.

[2] The European VLBI Network is a joint facility of European, Chinese, South African and other radio astronomy institutes funded by their national research councils.

[3] The GSFC ICRF2 VLBI Source Position Catalog.

[4] http://irsa.ipac.caltech.edu/data/SPITZER/GLIMPSE/

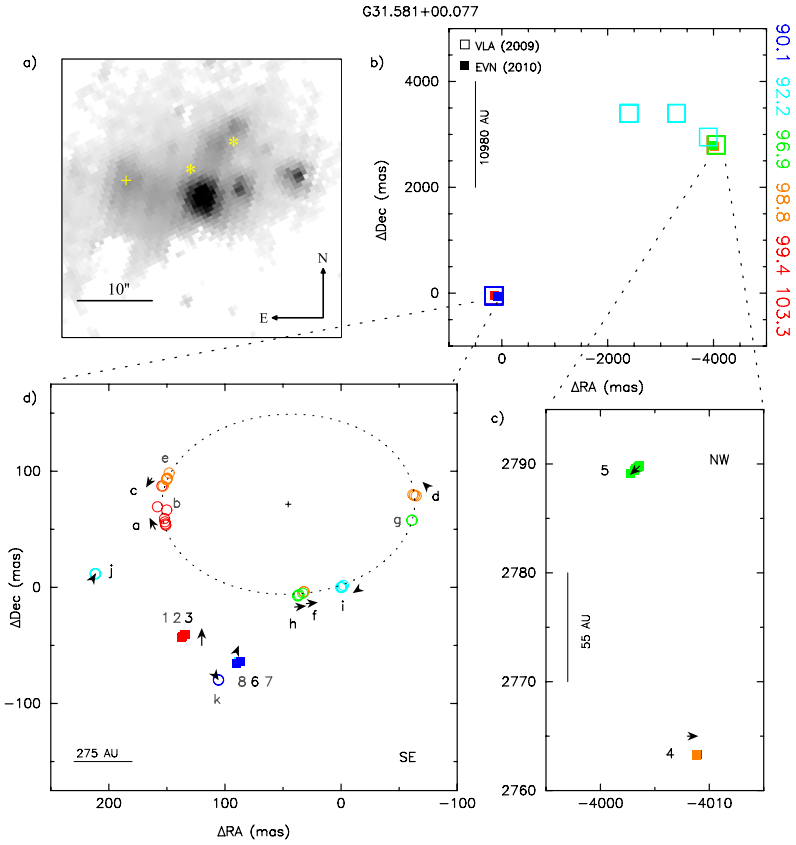

Fig. 1. G31.581+00.077. **a)** *Spitzer* GLIMPSE 4.5–3.6 μm excess image overlaid with the water maser positions (yellow asterisks) from the EVN observation and H II region (yellow cross) detected by Bartkiewicz et al. (2009). **b)** Shows the distribution of water masers observed with the EVN (filled squares) from this paper and the VLA (open squares) from Bartkiewicz et al. (2011). The colours of the symbols relate to the LSR velocities as indicated on the right-hand side of the plot. The origin of the map is the position of the brightest 6.7 GHz methanol maser spot (Bartkiewicz et al. 2009) (see also Table 1). **c)** Shows an enlargement of the north-western (NW) water masers. **d)** Shows an enlargement of the south-eastern (SE) water masers together with the distribution of the 6.7 GHz methanol masers, marked by open circles, from Bartkiewicz et al. (2009). In **c)** and **d)**, the arrows represent the velocity gradients (from blue- to red-shifted LSR velocities) detected within individual cloud. The black numbers and letters correspond to the clouds with internal velocity gradients, while the grey ones correspond to the clouds without internal velocity gradients (Table 3).

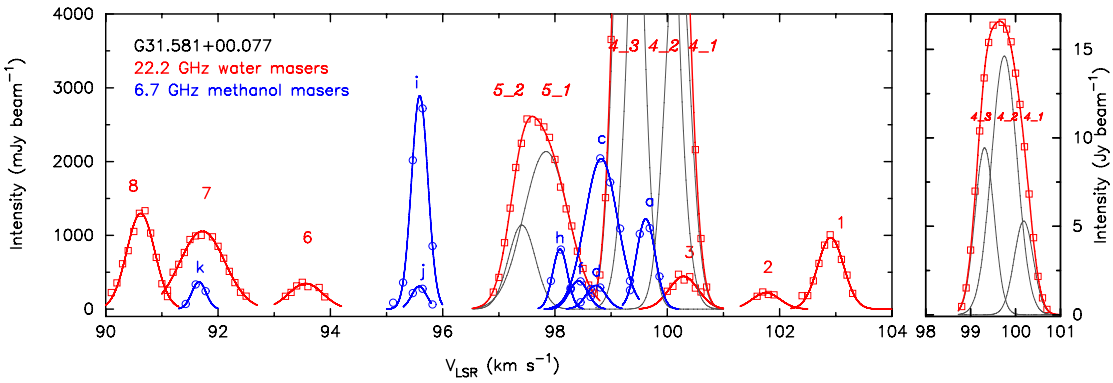

Fig. 2. Individual component spectra with Gaussian velocity profiles of 22.2 GHz water masers (red squares and lines) and 6.7 GHz methanol masers (blue circles and lines) towards G31.581+00.077 detected using the EVN in 2010 and 2007, respectively. The numbers and letters correspond to the cloud labels as given in Table 1 and Fig. 1. The grey lines show individual Gaussian profiles fitted to the blended features. The clouds with only two single spots are not marked to improve the clarity of the figure (i.e., clouds **b**, **e**, **g**).

The SE region is divided into the cluster of clouds *1*, *2*, and *3* separated by 50 mas from the cluster of clouds *6*, *7*, and *8* (Fig. 1). The clouds in the SE region show Gaussian velocity profiles with FWHM linewidths of 0.54–0.94 km s^{-1}. Their projected sizes are 0.07–0.47 mas, which correspond to 0.9–2.6 AU for the adopted distance of 5.5 kpc. The brightness temperature is 0.24–1.38 $\times$ 10^9 K. We note that clouds *3* and *6* show the velocity gradient of 1.3–1.8 km s^{-1} mas^{-1} oriented along PAs of 1° and −23°, respectively. It is remarkable that the two clusters of clouds (*1*, *2*, *3* and *6*, *7*, *8*) appear very close in space (Table 1) forming arc-like filaments of projected length of 4 and 3.2 mas corresponding to 22 and 18 AU, respectively, and elongated at PA = −58°. The closest clouds *3* and *6* are separated by 285 AU and a velocity difference of 6.7 km s^{-1}. The mean linear

Table 1. List of 22.2 GHz water maser clouds as found in EVN observations towards G31.581+00.077.

Cloud	V_{LSR} (km s^{-1})	ΔRA (mas)	ΔDec (mas)	S_p (mJy beam^{-1})	Number of spots
1	102.9	137.78	−43.02	1008	10
2	101.7	136.79	−42.58	233	4
3	100.2	134.57	−40.69	472	7
4	99.7	−4008.86	2763.28	16534	20
5	97.5	−4003.61	2789.88	2577	18
6	93.5	88.23	−64.04	363	7
7	91.7	86.79	−63.97	1000	14
8	90.7	89.65	−65.48	1333	11

Notes. The (0, 0) point corresponds to the position of the brightest *methanol* maser in this source (Bartkiewicz et al. 2009): RA = $18^h48^m41\overset{s}{.}94108$, Dec = $-01°10'02\overset{''}{.}5281$ (J2000).

Table 2. List of 22.2 GHz water maser clouds as observed using EVN towards G33.641−00.228.

Cloud	V_{LSR} (km s^{-1}	ΔRA (mas)	ΔDec (mas)	S_p (mJy beam^{-1})	Number of spots
1	58.1	87.77	−271.39	174	3
2	57.3	17.79	−8.96	606	7
3	56.1	46.98	−279.33	157	4
4	54.8	48.62	−277.37	263	3
5	55.1	48.65	−277.49	118	2
6	54.5	48.69	−277.40	217	2

Notes. The (0, 0) point correspond to the brightest *methanol* maser in this source (Bartkiewicz et al. 2009): RA = $18^h53^m32\overset{s}{.}563$, Dec = $+00°31'39\overset{''}{.}180$ (J2000).

separation between the two clusters along PA = 65° is 310 ± 8 AU, while the velocity spread is 13.2 km s^{-1}. The velocities of the two filaments are approximately symmetric with the regard of the systemic velocity of 96.0 km s^{-1} (Szymczak et al. 2007). The two SE filaments are likely signatures of flattened shock surfaces (Torrelles et al. 2001). We found that the water cloud *7* coincides within ±0.1 km s^{-1} with the methanol maser cloud *k*, while the spatial separation is 24.4 mas which corresponds to the projected distance of 134 AU. Although these two lines were observed within a time span of three years their separation seems to be real. This confirms that the water and methanol masers probe different parts of the environment of young massive stars (e.g., Beuther et al. 2002; Sanna et al. 2010a,b) because of the different pumping mechanisms affecting both species (Elitzur et al. 1989; Cragg et al. 2005).

The NW region of elongation of 26 mas is composed of two clouds *4* and *5* of brightness temperatures of 2.7−17.1 × 10^9 K (Table 3). Their velocity profiles are obviously asymmetric and nicely fitted by the sums of three and two Gaussian components (Fig. 2) of FWHM linewidth of 0.5−0.9 km s^{-1}. The velocities of the NW water maser emission largely coincide with those of the methanol masers but their linear separation is about 27 000 AU. The map of 4.5–3.6 μm emission excess (Fig. 1), which possibly traces shocked molecular gas in outflows from massive stars (e.g., Davies et al. 2007), shows that the SE and NW maser clusters lie in a very complex region. Both maser clusters are likely associated with different powering sources.

The comparison of our maps with those obtained about 14 months earlier with the VLA in a CnB configuration (Bartkiewicz et al. 2011) implies that the cloud *1* coincides to within 13 mas, the cloud *4* to within 56 mas, and the cloud *7* to within 64 mas with the matching VLA spots. The emission seen with the VLA from three components located ∼1−2″ eastward of the clouds *4* and *5* is not detected. We also note that the water maser components detected have very similar amplitudes in both EVN and VLA observations.

3.2. G33.641−00.228

Twenty-one water maser spots were detected in the velocity range of 54.4−57.6 km s^{-1} over the north-south elongated area 50 × 280 mas^2 close to the phase centre (Fig. 3). Using the above-mentioned procedure, we found four maser clouds where the emission is seen in at least three contiguous spectral channels. There are also two other clouds (*5* and *6*) that do not obey this criterion but seem to be real (Table 2). All but one of the cloud are in the southward cluster at a distance ∼270 mas from the phase centre. This filament cluster of size 41.6 mas is aligned along a PA of 78°. For the adopted distance of 3.8 kpc, the corresponding linear scales are 1020 AU and 157 AU. The clouds *1*−*4* in the southern cluster have Gaussian profiles with FWHM linewidths of 0.25−0.88 km s^{-1}. We note that none of the water clouds have an internal velocity gradient. The linear size of the individual clouds is 0.3−1.0 AU and the brightness temperature is 0.12−0.27 × 10^9 K (Table 3).

The strongest emission (T_b = 0.63 × 10^{9}K) comes from cloud *2*, which is a blend of two Gaussian components (Fig. 4). Cloud *2* is ∼20 mas (75 AU) away from the brightest methanol maser clouds *a* and *r* and differ in terms of velocity by 1.5 km s^{-1}. This is probably the first such tight association of methanol and water masers. We note that the emission of cloud *2* is blue-shifted by 4.2 km s^{-1} and that of cloud *a* is red-shifted by 1.2 km s^{-1} relative to the systemic velocity of 61.5 km s^{-1} (Szymczak et al. 2007). It is therefore possible that these clouds signpost a shock front in which the water emission originates behind the front, while the methanol emission (cloud *a*) appears outside of the shock interface in the infalling gas.

The image of the 4.5 μm−3.6 μm emission excess (Fig. 3) shows that the water maser emission is located 1″.2 to the south-east of single mid-infrared object. This is likely the source powering the outflow along a PA of 165° traced by the water masers.

The positions of the clouds *2*, *3*, *4* and *6* differ by about 92 mas from the VLA positions of the matching clouds (Bartkiewicz et al. 2011), which is well within the ∼150 mas accuracy of the CnB configuration VLA data. A weak (<0.9 Jy) red-shifted emission in the velocity range of 83.8−85.1 km s^{-1} seen with the VLA towards cloud *2* (Fig. 1) was not recovered in the VLBI observation. The brightness of the emission from cloud *2* determined in the EVN observation is only slightly lower than that measured with the VLA. In contrast, the maser spots from the southern region (clouds *1*, *3*−*6*) are about ten times weaker in the EVN maps that may suggest the presence of diffuse and/or highly variable emission.

4. Discussion

4.1. Maser environments

The *Spitzer* GLIMPSE map (Fig. 1) clearly indicates that the source G31.581+00.077 lies in a large (35″×25″) complex area with an 4.5 μm emission excess in the form of clumped and diffuse structures. This extended emission is proposed to be a tracer of shocked gas from regions where outflowing gas interacts with the surrounding medium (Davis et al. 2007; Cyganowski et al. 2009). The ^{13}CO(1−0) spectrum obtained with a 46″ beam

Table 3. Parameters of 22.2 GHz water and 6.7 GHz methanol maser clouds.

Cloud	S_p (mJy beam^{-1})	S_{fit} (mJy beam^{-1})	V_{fit} (km s^{-1})	$FWHM$ (km s^{-1})	L_{proj} (mas)	L_{proj} (AU)^i	V_{grad} (km s^{-1} mas^{-1})	V_{grad} (km s^{-1} AU^{-1})^i	T_b ($\times 10^8$ K)
G31.581+00.077					22.2 GHz water masers				
1	1008	969	102.9	0.54	0.17	0.93	–	–	10.4
2	233	221	101.8	0.58	0.07	0.38	–	–	2.4
3	472	444	100.3	0.61	0.47	2.58	1.3	0.24	4.9
4	16534	–	–	–	0.10	0.55	21.2	3.84	170.8
4_1	–	5302	100.2	0.50	–	–	–	–	–
4_2	–	14630	99.8	0.67	–	–	–	–	–
4_3	–	9445	99.3	0.50	–	–	–	–	–
5	2577	–	–	–	1.17	6.42	1.8	0.33	26.6
5_1	–	2137	97.8	0.93	–	–	–	–	–
5_2	–	1140	97.4	0.57	–	–	–	–	–
6	363	347	93.6	0.72	0.35	1.92	2.0	0.36	3.8
7	1000	1057	91.7	0.94	0.36	1.98	–	–	10.3
8	1333	1297	90.6	0.58	0.24	1.32	–	–	13.8
					6.7 GHz methanol masers				
a	1099	1223	99.6	0.39	5.8	31.84	0.09	0.016	3.4
b*	358	–	–	–	–	–	–	–	1.1
c	2045	2039	98.8	0.68	7.4	40.63	0.07	0.013	6.4
d	292	321	98.7	0.41	2.9	15.92	0.12	0.022	0.9
e*	493	–	–	–	–	–	–	–	1.5
f	376	386	98.4	0.39	1.6	8.78	0.23	0.042	1.2
g*	349	–	–	–	–	–	–	–	1.1
h	809	814	98.1	0.31	2.0	10.98	0.18	0.033	2.5
i	2722	2891	95.6	0.35	2.8	15.37	0.25	0.046	8.5
j	276	308	95.6	0.31	0.7	4	0.72	0.088	0.9
k	333	371	91.7	0.30	3.0	16.3	0.12	0.022	1.0
G33.641−00.228					22.2 GHz water masers				
1	174	177	58.1	0.25	0.11	0.42	–	–	1.8
2	606	–	–	–	0.16	0.60	–	–	6.3
2_1	–	326	57.3	0.50	–	–	–	–	–
2_2	–	328	57.3	0.08	–	–	–	–	–
3	157	158	56.3	0.88	0.27	1.02	–	–	1.6
4	263	263	54.8	0.34	0.08	0.30	–	–	2.7
5*	118	–	–	–	–	–	–	–	1.2
6*	217	–	–	–	–	–	–	–	2.2
					6.7 GHz methanol masers				
a	20690	–	–	–	6.7	25.26	0.20	0.053	64.8
a_1	–	9670	62.9	0.49	–	–	–	–	–
a_2	–	17826	62.6	0.22	–	–	–	–	–
a_3	–	5038	62.3	0.23	–	–	–	–	–
b	1090	1124	63.1	0.3	3.3	12.44	–	–	3.4
c	893	811	62.2	0.6	9.0	33.93	0.07	0.019	2.8
d	365	358	61.9	0.4	5.8	21.87	–	–	1.1
e**	207	–	–	–	1.3	7.92	–	–	0.6
f	10447	–	–	–	7.5	28.28	0.07	0.019	32.7
f_1	–	6913	61.0	0.19	–	–	–	–	–
f_2	–	7184	60.8	0.33	–	–	–	–	–
g**	356	–	–	–	0.5	10.56	–	–	1.1
h	1672	1716	60.9	0.30	1.2	4.52	–	–	5.2
i**	2280	–	–	–	3.3	22.9	–	–	7.1
j	20402	21448	60.3	0.30	2.9	10.93	0.21	0.056	63.9
k	12260	12665	59.8	0.22	6.0	22.62	0.06	0.016	38.4
l	4105	4362	59.6	0.26	10.9	41.10	–	–	12.9
n*	109	–	–	–	–	–	–	–	0.3
p*	176	–	–	–	–	–	–	–	0.6
r	28300	29569	58.8	0.30	1.2	4.52	–	–	88.6

Notes. (*) The emission only in two channels. (**) More than two spots in a cloud, but no Gaussian characteristic of its spectrum. (i) Assuming the near kinematic distances, 5.5 kpc and 3.8 kpc for G31.581+00.077 and G33.641−00.228, respectively (Sect. 3).

(Urquhart et al. 2008) towards the position 31.5808+0.0757 has two Gaussian components centred at 96.2 and 109.8 km s^{-1}. A weak emission line is clearly detected in the range of 85 to 105 km s^{-1}, i.e., in the wings of the first component suggests the presence of outflows. A signature of ordered motions also appears in the HCO$^+$(1−0) spectrum (Szymczak et al. 2007), where in this slightly asymmetric profile the strongest emission is blueward of the source systemic velocity and can be interpreted as the result of infall (e.g., Fuller et al. 2005). We then find 9.″2 east of the SE water maser an H II region of

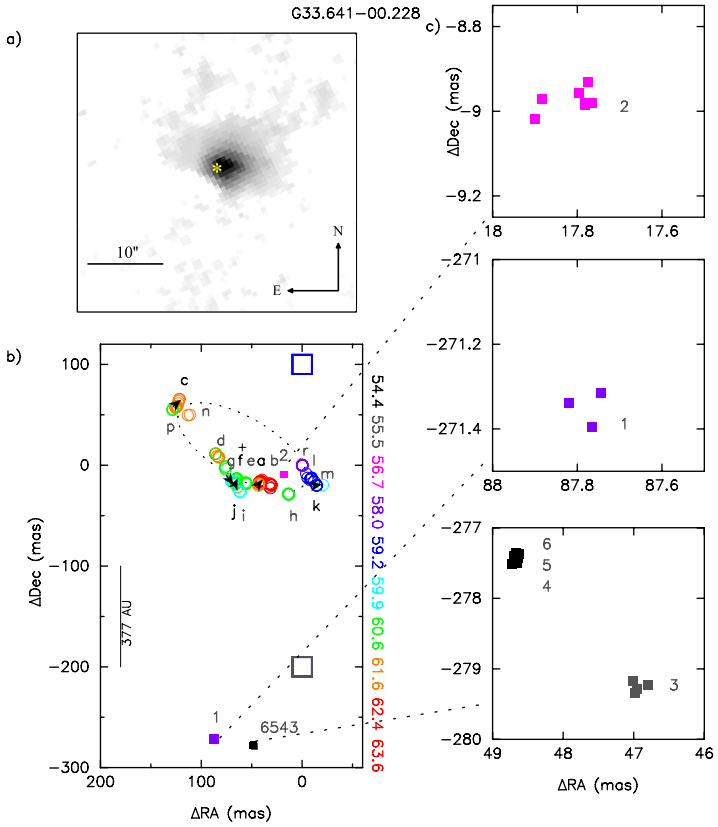

Fig. 3. Same as Fig. 1 but for G33.641−00.228.

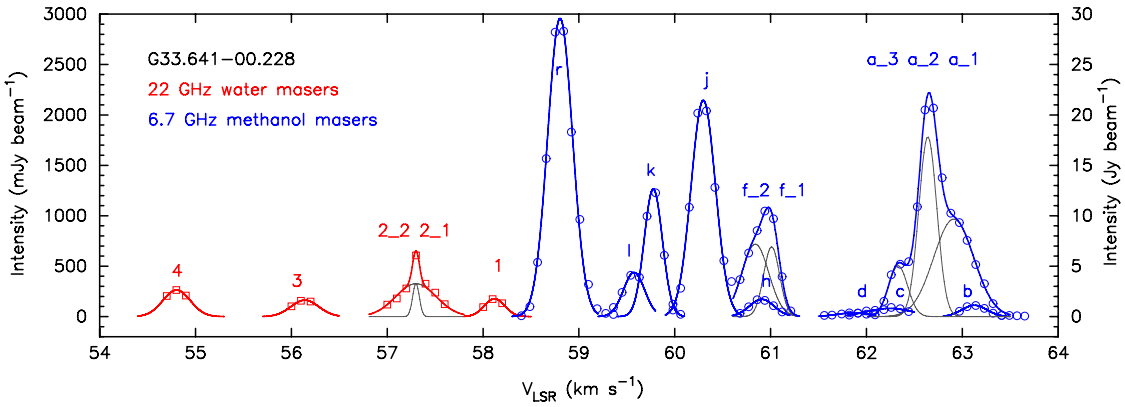

Fig. 4. Same as Fig. 2 but for G33.641−00.228. The scale on the left side describes the water maser intensity, while the right side corresponds to the methanol maser intensity. The clouds with only two single spots or without Gaussian characteristic are not marked for the clarity of the figure (i.e., clouds *5*, *6*, *e*, *g*, *i*, *n*, *p*).

flux density 10.3 and 15 mJy at 5 GHz (White et al. 2005) and 8.4 GHz (Bartkiewicz et al. 2009), respectively. This continuum source coincides to within 0.″6 with a clump of 3.6–4.5 μm emission excess (Fig. 1). The NW water masers are located at the borders of two clumps of excited gas, and their powering source is unclear although it seems unlikely that the SE and NW masers are associated with the same central object. A comparison of the present EVN maps with those obtained with the VLA 14 months earlier (Bartkiewicz et al. 2011) implies that there is a lack of water masers eastward of the NW clouds (Fig. 1). It is likely that these are diffuse and low intensity masers resolved out with the EVN beam. The spectrum obtained with a 40″ beam sometime between November 2009 and December 2010 (Urquhart et al. 2011) indicates that the peak flux density of 125 Jy at 99.7 km s^{-1} is about one order of magnitude higher than that measured with the EVN. We suggest that the water masers of G31.581+00.077 are produced by different young stellar objects in a complex region composed of at least a few high-mass stars well-signposted by the radio continuum and the methanol and water masers.

The water maser in G33.641−00.228 lies only 1.″2 southeastward of the maximum of the 3.6–4.5 μm emission excess of cometary-like morphology (Fig. 3). The HCO$^+$(1−0) spectrum obtained towards the position 33.648−0.224 (Szymczak et al. 2007) shows a small dip near 61.5 km s^{-1} and a slight redward asymmetry that is indicative of outflow motions. The less optically thin H^{13}CO$^+$(1−0) transition is detected as marginal red-shifted emission, which is consistent with an outflow. In the region where the OH 1665, 1667, and 1720 MHz masers

were detected (Szymczak & Gérard 2004) and all of them peak at 60.2 km s^{-1}. The strongest 1720 MHz emission and a broad (7.4 km s^{-1}) 1667 MHz absorption profile near 56.2 km s^{-1} are indicative of shock fronts and a continuum background source, respectively. No continuum emission at 8.4 GHz was detected with a $3\sigma_{\rm rms}$ limit of 0.15 mJy beam^{-1} (Bartkiewicz et al. 2009). A weak (~20 mJy) 8.6 GHz hydrogen radio recombination-line near 102.9 km s^{-1} detected at position G033.645−0.227 (Anderson et al. 2011) differs so greatly in terms of velocity from the water masers that this may be a chance projection that is unassociated with the methanol and water masers. We argue that the water masers of G33.641−00.228 as well as the associated methanol and hydroxyl masers are excited by individual high-mass stars.

4.2. Physical parameters of circumstellar medium

Lower limits to the brightness temperature of the SE water maser components associated with G31.581+00.077 are always lower than 1.4×10^9 K, while the measured linewidths range from 0.54 to 0.94 km s^{-1} are quite commonly in the star-forming sources (e.g., Goldreich & Kwan 1974; Surcis et al. 2011a, 2011b). Since the kinetic temperature of the masing gas might be expected to be about 400 K (Elitzur et al. 1989), the intrinsic thermal linewidth given by $\Delta v_{\rm FWHM} = 2.35482\times\sqrt{kT_{\rm k}/m}$, where $T_{\rm k}$ is a kinetic temperature, k the Boltzmann constant, and m is a molecular mass should be ~1 km s^{-1}. This value is larger than the observed linewidths and suggests that the masers are unsaturated. In the same volume of gas where the water maser cloud *7* and the methanol maser cloud *k* appear to coincide (Fig. 1), the methanol thermal linewidth would be 0.75 km s^{-1}, whereas the measured value is 0.30 km s^{-1}. The narrowing of the line profile is expected when the maser is unsaturated. Detailed calculations have shown that in one of the strongest known methanol sources NGC 7538 about 92% of the components are unsaturated (Surcis et al. 2011b). In the source G33.641−00.228, the observed linewidths of methanol components are generally narrower than in G31.581+00.077, which suggests that the maser is also unsaturated in this region.

The mas-scale velocity gradients in both lines are observed in G31.581+00.077. We note that the velocity gradient at 22 GHz is about one order of magnitude higher than at 6.7 GHz (Table 3). Extensive discussion of the velocity gradients for methanol masers by Moscadelli et al. (2011b) suggests that there is a kinematical interpretation of their origin. We note that the methanol maser gradients in both targets can reflect the ordered motions on scales of 10−60 AU. Large velocity gradients for water masers in G31.581+00.077 suggest that they are related to the outflow motions with velocities larger than 50 km s^{-1} (see Sect. 4.3).

4.3. Kinematic models

The two sources investigated in this study possibly belong to a group of objects where a ring-like or arc-like methanol maser distribution traces a circumstellar disc/torus around a high-mass young stellar object, whereas the water maser distribution is orthogonal to the major axis of the methanol structure (Bartkiewicz et al. 2011). Furthermore, these objects are not associated with detectable continuum emission at cm wavelengths (Bartkiewicz et al. 2009) and may represent an early stage of evolution. The new EVN observations of both sources have shown that all of the individual water maser spots detected previously with the VLA (Bartkiewicz et al. 2011) unfold into complex and filament structures of sizes 18−160 AU. To examine a disc-outflow scenario in the two sources, we used a model of a rotating and expanding thin disc (Uscanga et al. 2008) for the methanol masers and a model of the outflow (Moscadelli et al. 2000) for the water masers. Detailed descriptions of the modelling are given in the above cited works, and elsewhere for methanol masers in discs (Bartkiewicz et al. 2009) and outflows (Bartkiewicz et al. 2006). We note that in the following we analyse the new water maser data with the methanol maser data obtained 3−7 years earlier (Bartkiewicz et al. 2009). However, our inspection of a few sources published so far and systematic EVN monitoring demonstrate that the overall methanol maser morphologies are stable on a scale time of 6−8 years (Bartkiewicz et al., in prep.).

Table 4. Parameters derived by fitting the kinematics of the rotating and expanding disc model.

Source	$V_{\rm rot}$ (km s^{-1})	$V_{\rm exp}$ (km s^{-1})	$V^1_{\rm sys}$ (km s^{-1})	i (°)	$\chi^2_{\rm V}$
G31.581+00.077					
	0.90	1.71	98.54	77.5	134
G33.641−00.228					
D1	0.84	−1.05	61.00	30.0	184
D2	3.72	1.74	58.40	−30.0	222

Notes. The signs + and − of the rotation and expansion velocities refer to the clockwise or anti-clockwise rotation and outflow or inflow for positive i. Both rotation and flow are reversed in the case of negative i. For each source, both signs together with the sign of i could be reversed since our model does not give the directions unambiguously. In the case of G33.641−00.228, two model fits are presented as described in Sect. 4.3. [(1)] Systemic velocity.

In Tables 4 and 5, we summarize the best-fit values of both models. For the rotating and expanding thin disc, the rotation ($V_{\rm rot}$), expansion ($V_{\rm exp}$), and systemic ($V_{\rm sys}$) velocities as well as the inclination angle, i, i.e., the angle between the line-of-sight and the normal to the ring plane defined to be $i = \arccos(\frac{b}{a})$ is given for each source. The solutions were based on the minimization of the $\chi^2_{\rm V}$ function given by Eq. (8) in Uscanga et al. (2008). The outflow model for water masers is characterized by the vertex of the cone ($X_{\rm o}$, $Y_{\rm o}$), the x-axis coinciding with the projection of the outflow on the plane of the sky at the position angle PA, the inclination angle between the outflow axis and the line-of-sight (i.e., the z-axis) Ψ, and the opening angle of the outflow/cone 2θ. The systemic LSR velocities, $V_{\rm c}$, were assumed to be the same as given in Sect. 3. The χ^2 function was assumed to be expressed as in Eq. (3) of Moscadelli et al. (2000).

The methanol emission in G31.581+00.077 is most accurately reproduced by the model where the powering source is at the centre of the best-fit ellipse and the rotation velocity of 0.9 km s^{-1} is a factor of two lower than the expansion velocity (Table 4, Fig. 5). These values are typical of the class of ring-like methanol masers (Bartkiewicz et al. 2009) and suggest that the methanol structure of ~1000 AU diameter cannot be interpreted as a Keplerian disc. It is instead proposed that the methanol masers arise on the interface region between a large-scale accretion flow and a stellar disc (van Langevelde et al. 2010; Torstensson et al. 2011). We also note that the best-fit systemic velocity of 98.54 km s^{-1} corresponds well to that estimated from molecular lines (Sect. 3.1). The SE water emission is reasonably well-fitted by two different models. In the first

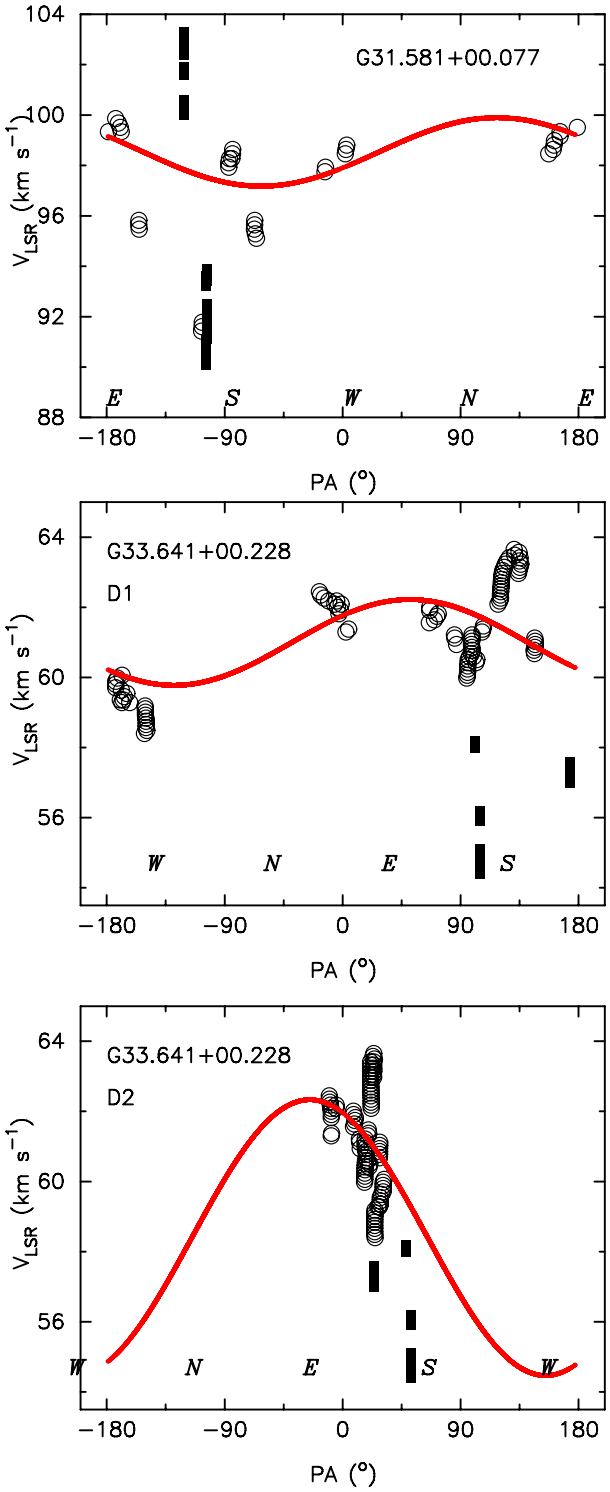

Fig. 5. Velocity of the methanol maser spots (open circles) in G31.581+00.077 and G33.641+00.228 versus azimuth angle measured from the major axis. The sinusoidal line represents the best-fit kinematical model of a rotating and expanding disc of infinitesimal thickness to the methanol spots with the parameters listed in Table 4. For completeness, the water maser spots are shown as squares. In a case of G33.641+00.228 two kinematical models are presented for a powering source located as follow: D1 – in the centre of the best-fitted ellipse, D2 – at the MIR position.

model, O1, the vertex of the cone with $2\theta = 30°$ coincides with the centre of the methanol ellipse within 25 mas and the velocity of masers is 77 km s^{-1} (Table 5, Fig. 6). We argue that this fit is consistent with the outflow scenario.

Table 5. Parameters derived from fitting the biconical outflow model of Moscadelli et al. (2000).

Source	X_o (mas)	Y_o (mas)	V_o^1 (km s^{-1})	PA (°)	θ (°)	Ψ (°)	χ^2
G31.581+00.077							
O1	72	68	−77.0	−16	15	83	1.7
O2	110	−46	7.7	67	17	45	0.7
G33.641−00.228	15	5	15.2	16	9	67	0.1

Notes. In the case of G31.581+00.077, two model fits are presented as described in Sect. 4.3. [(1)] Constant velocity of a maser spot, + for a direction radially outward from the central star.

As we failed to identify any mid-infrared (MIR) counterpart to the centre of the methanol ellipse as a powering source of the methanol structure and perpendicular to the water maser outflow, we propose an alternative model. This second model, O2, assumes that the position of the cone vertex is just between the red-shifted and blue-shifted voids of SE water masers. The best-fit velocity of the outflow is ∼8 km s^{-1}, while the projection of the axis outflow onto the plane of the sky is roughly parallel to the main axis of the methanol structure (Table 5, Fig. 6). In star forming regions, different centres of activity are reported on scale sizes of a few to several hundred AUs (e.g., Torrelles et al. 2001, 2011). The proper motion studies of G31.581+00.077 can clearly provide conclusive evidence for or against this hypothesis.

In the case of methanol masers in G33.641−00.228, we present the two kinematical models for a powering source located at the centre of the best-fit ellipse (ΔRA, ΔDec) = (59 mas,17 mas) and that located at the MIR position (−495 mas, 380 mas). In the first model, D1, the infall velocity of about 1 km s^{-1} is slightly higher than the rotation velocity (Table 4). The structure of water masers is fitted by a narrow ouflow of $2\theta = 18°$ and velocity of 15 km s^{-1} (Table 5, Fig. 6). It is consistent with a jet-like outflow of water masers roughly perpendicular to the main axis of methanol structure. In the second model, D2, the visible methanol structure is only a small part of the disc radius of ∼1900 AU and the rotation velocity of 3.7 km s^{-1} (Table 4), which implies that the enclosed mass is about 30 $M_\odot$. In this case, the water masers may trace the wind gas from a disc.

We note that the kinematic models are unable to accurately reproduce the observed structures of the methanol and water masers in both targets, and that only measurements of the proper motions of maser spots of the two species can unambiguously constrain the proposed scenarios.

5. Conclusions

We have carried out high-angular resolution studies of the 22.2 GHz of water maser line towards two methanol maser sources G31.581+00.077 and G33.641−00.228 using the EVN. Although their morphologies did not differ significantly from the previous VLA results, the astrometry at the mas level and the properties of the maser clusters could be estimated owing to the high-angular and spectral resolution. In total, we detected eight and six water maser clouds towards G31.581+00.077 and G33.641−00.228, respectively. In the first target, the water maser components are associated with different centres of star-forming activity, and the components associated with the methanol ring-like structure possibly trace the outflow. In the

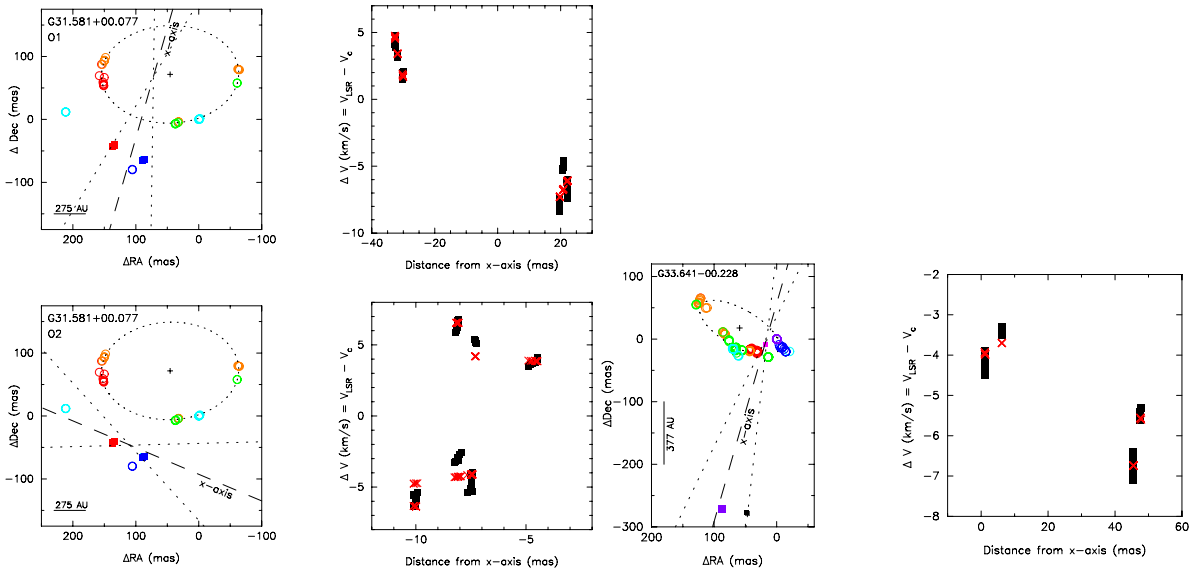

Fig. 6. Outflow models fitted to water (squares) in G31.581+00.077 and G33.641+00.228 according to the model of Moscadelli et al. (2000). The relevant parameters are listed in Table 5. The *right panel* presents a comparison of obtained data (squares) vs. model (crosses). V_c is the systemic LSR velocity as given in Sect. 3.

source G33.641−00.228, southern water masers possibly trace a wind from a disc. The kinematic models containing ring-like or arc-like methanol maser structures are able to trace a circumstellar disc/torus around a high-mass young stellar object, whereas the water maser distribution is orthogonal to the major axis of the applied methanol structure and poorly constrained by the present data. The present studies show that the two sources are good targets for proper motion studies in order to understand more clearly the kinematics of gas in the environments of high-mass stellar objects. They also encourage us to extend the multi-epoch EVN observations for a whole sample.

Acknowledgements. A.B. and M.S. acknowledge support by the Polish Ministry of Science and Higher Education through grant N N203 386937. This work has also been supported by the European Community Framework Programme 7, Advanced Radio Astronomy in Europe, grant agreement No.: 227290.

References

Anderson, L. D., Bania, T. M., Balser, D. S., & Rood, R. T. 2011, ApJS, 194, 32
Bartkiewicz, A., Szymczak, M., & van Langevelde, H.J. 2006, in Proc. 8th European VLBI Network Symposium, Torun, 39
Bartkiewicz, A., Szymczak, M., van Langevelde, H. J., Richards, A. M. S., & Pihlström, Y. M. 2009, A&A, 502, 155
Bartkiewicz, A., Szymczak, M., Pihlström, Y. M., et al. 2011, A&A, 525, A120
Beuther, H., Walsh, A., Schilke, P., et al. 2002, A&A, 390, 289
Caswell, J. L., Vaile, R. A., Ellingsen, S. P., Whiteoak, J. B., & Norris, R. P. 1995, MNRAS, 272, 96
Chambers, E. T., Yusef-Zadeh, F., & Roberts, D. 2011, ApJ, 733, 42
Cragg, D. M., Sobolev, A. M., & Godfrey, P. D. 2005, MNRAS, 360, 533
Cyganowski, C. J., Brogan, C. L., Hunter, T. R., & Churchwell, E. 2009, ApJ, 702, 1615
Davis, C. J., Kumar, M. S. N., Sandell, G., et al. 2007, MNRAS, 374, 29
De Buizer, J. M. 2003, MNRAS, 341, 277
Diamond, P. J., Garrington, S. T., Gunn, A. G., et al. 2003, MERLIN User Guide, Version 3, www.merlin.ac.uk
Dodson, R., Ojha, R., & Ellingsen, S. P. 2004, MNRAS, 351, 779
Elitzur, M., Hollenbach, D. J., & McKee, C. F. 1989, ApJ, 346, 983
Fazio, G. G., Hora, J. L., Allen, L. E., et al. 2004, ApJS, 154, 10
Fuller, G. A., Williams, S. J., & Sridharan, T. K. 2005, A&A, 442, 949
Garay, G., & Lizano, S. 1999, PASP, 111, 1049
Goddi, C., Moscadelli, L., Sanna, A., Cesaroni, R., & Minier, V. 2007, A&A, 461, 1027
Goldreich, P., & Kwan, J. 1974, ApJ, 190, 27
Menten, K. M. 1991, ApJ, 380, L75
Minier, V., Booth, R. S., & Conway, J. E. 2000, A&A, 362, 1093
Moscadelli, L., Cesaroni, R., & Rioja, M. J. 2000, A&A, 360, 663
Moscadelli, L., Goddi, C., Cesaroni, R., Beltrán, M. T., & Furuya, R. S. 2007, A&A, 472, 867
Moscadelli, L., Cesaroni, R., Rioja, M. J., Dodson, R., & Reid, M. J. 2011a, A&A, 526, A66
Moscadelli, L., Sanna, A., & Goddi, C. 2011b, A&A, 536, A38
Norris, R. P., Byleveld, S. E., Diamond, P. J., et al. 1998, ApJ, 508, 275
Pandian, J. D., Momjian, E., Xu, Y., Menten, K. M., & Goldsmith, P. F. 2011, ApJ, 730, 55
Philips, C. J., Norris, R. P., Ellingsen, S. P., & McCulloch, P. M. 1998, MNRAS, 300, 1131
Reid, M. J., Menten, K. M., Zheng, X. W., et al. 2009, ApJ, 700, 13
Sanna, A., Moscadelli, L., Cesaroni, R., et al. 2010a, A&A, 517, A71
Sanna, A., Moscadelli, L., Cesaroni, R., et al. 2010b, A&A, 517, A78
Sobolev, A. M., Cragg, D. M., & Godfrey, P. D. 1997, A&A, 324, 211
Sridharan, T. K., Beuther, H., Schilke, P., Menten, K. M., & Wyrowski, F. 2002, ApJ, 566, 931
Surcis, G., Vlemmings, W. H. T., Curiel, S., et al. 2011a, A&A, 527, A48
Surcis, G., Vlemmings, W. H. T., Torres, R. M., van Langevelde, H. J., & Hutawarakorn Kramer, B. 2011b, A&A, 533, A47
Szymczak, M., & Gérard, E. 2004, A&A, 414, 235
Szymczak, M., Hrynek, G., & Kus, A. J. 2000, A&AS, 143, 269
Szymczak, M., Kus, A. J., Hrynek, G., Kepa, A., & Pazderski, E. 2002, A&A, 392, 277
Szymczak, M., Pillai, T., & Menten, K. M. 2005, A&A, 434, 613
Szymczak, M., Bartkiewicz, A., & Richards, A. M. S. 2007, A&A, 468, 617
Torrelles, J. M., Patel, N. A., Gómez, J., et al. 2001, ApJ, 560, 853
Torrelles, J. M., Patel, N. A., Curiel, S., et al. 2011, MNRAS, 410, 627
Torstensson, K. J. E., van Langevelde, H. J., Vlemmings, W. H. T., & Bourke, S. 2011, A&A, 526, A38
Uscanga, L., Gomez, Y., Raga, A. C., et al. 2008, MNRAS, 390, 1127
Urquhart, J. S., Busfield, A. L., Hoare, M. G., et al. 2008, A&A, 487, 253
Urquhart, J. S., Hoare, M. G., Purcell, C. R., et al. 2009, A&A, 501, 539
Urquhart, J. S., Hoare, M. G., Lumsden, S. L., et al. 2010, A&A, 507, 795
Urquhart, J. S., Moore, T. J. T., Hoare, M. G., et al. 2011, MNRAS, 410, 1237
van Langevelde, H. J., Torstensson, K. J. E., Bartkiewicz, A., et al. 2010, in Proc. 10th European VLBI Network Symposium, Manchester, 2
Walsh, A. J., Burton, M. G., Hyland, A. R., & Robinson, G. 1998, MNRAS, 301, 640
Walsh, A. J., Breen, S. L., Britton, T., et al. 2011, MNRAS, 416, 176
White, R. L., Becker, R. H., & Helfand, D. J. 2005, AJ, 130, 586
Wrobel, J. M., & Walker, R. C. 1999, Lecture 9: Sensitivity in Synthesis Imaging in Radio Astronomy II, ASP Conf. Ser., 180, 171